e-Prime - Advances in Electrical Engineering, Electronics and Energy 10 (2024) 100852

Contents lists available at ScienceDirect

e-Prime - Advances in Electrical Engineering, Electronics and Energy

journal homepage: www.elsevier.com/locate/prime

Fast frequency response constrained stochastic scheduling of flexible loads in low inertia grids

Ashish Mathur, Sumit Nema, Vivek Prakash *, Jyotsna Singh

School of Automation, Banasthali Vidyapith 304022, India

ARTICLE INFO

Keywords:
Demand response
Distributed energy resources
Fast frequency response
Flexible loads
Load scheduling
Stochastic scheduling
Uncertainty modeling

ABSTRACT

This paper presents a modeling approach to address fast frequency response (FFR) requirements within a stochastic scheduling framework. The work integrates FFR response from flexible loads and propose advance modeling techniques to characterize renewable generation uncertainty. The study incorporates scenario-based uncertainty modeling to capture the inherent unpredictability of renewable energy resources (RES), enhancing the accuracy of scheduling in low inertia grids. Central to the proposed methodology is the integration of flexible loads such as interruptible loads (ILs), deferrable loads (DLs), and electric vehicles (EVs) strategically modeled to contribute to FFR capabilities. By embedding uncertainty modeling within the proposed stochastic scheduling framework, the research offers a comprehensive strategy to effectively handle the challenges posed by renewable generation fluctuations and reduces the RES curtailment. The paper underscores the significance of FFR in maintaining grid balancing, particularly in the presence of RES. The inclusion of flexible loads further contributes to enhancement of grid resilience by enabling rapid adjustments in response to frequency disturbances. The proposed framework not only accommodates renewable generation uncertainties but also leverages smart flexible loads to bolster FFR capabilities paving the way for a reliable and sustainable power systems.

1. Introduction

The traditional grids are challenged by a pressing need of distributed energy resources (DER), increasing demand of communities, growing threats to grid security and reliability together with concerns over expediting environmental disruption. As renewable sources continue to replace conventional synchronous generators, modern grids are becoming increasingly low inertia. This rapid shift has led to a reduction in the natural ability of the grid to respond to frequency deviations following disturbances [1]. In low-inertia grids, rapid frequency drops can increase the risk of system instability or even blackouts if not responded quickly. The issue of low inertia is a global challenge for the electrical utilities with aggressive renewable energy targets, such as Europe, North America, and parts of Asia, where the share of non-synchronous generation is growing rapidly [2]. Insufficient FFR can lead to cascading failures and widespread outages.

Consequently, current global policies have designed interventions to overcome these challenges and to facilitate grid modernization [3]. The grid modernization predominantly encourages integration of DER, thus transitioning traditional grids into smart grids. DER mainly composed renewable energy resources (RES) and energy storage system (ESS) including electric vehicles (EVs) [4,5]. However, increased penetration of intermittent and uncertain RES transforms the grid into low inertia smart grid. The low inertia grids are accountable for reduced frequency response traditionally delivered by conventional generators. The reduction in frequency response may impose challenge for grid such as high rate of change of frequency (RoCoF) which extends to high excursions in frequency after an inevitable contingency such sudden loss of generation or load [6].

To ensure reliability and security of the grid at the time of such contingency requires a fast frequency response (FFR). FFR can be defined as relatively fast (typically 1 s–2 s) balance between generation and load to stabilize frequency variations within prescribed limit after a contingency [2]. The technological advancement offered by smart grid can substantially contribute to enable FFR for rapid grid balancing services. The smart grid extends improved digital sensing and advance information and communication technologies for continuous monitoring of demand and generation. This facilitates incorporation of fast acting resources such as demand response (DR), RES, EVs and smart flexible loads for provision of FFR at the time of inevitable contingency particularly in low inertia grids [7]. The integration of EVs targets low

* Corresponding author.
E-mail addresses: ashishmathur@banasthali.in (A. Mathur), sumitnema@live.in (S. Nema), vivekprakash@banasthali.in (V. Prakash), jyotsnasingh@banasthali.in (J. Singh).

https://doi.org/10.1016/j.prime.2024.100852
Received 2 August 2024; Received in revised form 10 November 2024; Accepted 18 November 2024
Available online 26 November 2024

Nomenclature

Set

ω	Netload scenarios, indexed by ω
b, m	Buses or nodes (b,m)
ev	Electric vehicles (ev)
g	Generating units (g, where g ∈ [i,s,w]
i	Conventional generators(i)
pl	Parking lots (pl)
s	PV units (s)
T, t	Time (t)
w	Wind units (w)

Variables

Δf_t^{ss}	Deviation of frequency at time t (Hz)
$\theta_{b/m.t}$	Bus load angle at time t (degree)
f^{nad}	Frequency deviation at nadir for time t (Hz)
$f_{b,t}^{net}$	Total load demand at bus b for time t (MW)
$LS_{b,t,\omega}$	Load shedding at time t
$N_{pl,b,t}^{arv/dep}$	Arrival/departure of EVs to/from pl connected at b, at time t
$N_{ev,b,t}$	Total EVs connected to bus b at time t
$N_{pl,b,t}$	Total EVs at pl connected to b at time t
$P_{pl,t}^{ffr}$	Aggregated EVs FFR at pl for time t (MW)
$P_{i,t}^{pfr}$	Contribution of PFR from unit i at time t (MW)
$P_{i,t}^{res}$	Reserve contribution of unit i at time t (MW)
P_t^{rns}	Not served reserve at time t (MW)
$P_{bm,t}$	Flow of power in the line between buses b and m at time t (MW)
$P_{i,t}$	Generated power from i unit at time t (MW)
$RoCoF_t$	RoCoF at time t (Hz/s)
SI_t	Inertia of system for time t (MW-s/Hz)
$SOC_{ev,b,t}$	SOC of connected EVs at b for time t (KWh)
$SOE_{pl,b,t}$	Net Energy of pl at bus b during time t (KWh)
t_t^{nad}	Time to reach maximum under frequency at time t (s)

Binary

$\alpha_{i,t}$	Status(on/off) of unit i (1 for on otherwise 0)
$\beta/\gamma_{i,t}$	Start-up/shut down status of unit i (1 for start up, otherwise 0)
$\chi_{ev,t}^{char}$	Status of ev at time t
uIL_t	1 if IL responds at time interval t otherwise 0
$y_{i,t}$	1 if unit i is on at time t otherwise 0

Parameters

$\overline{\Delta f}^{SS}$	Frequency deviation at steady-state (Hz)
ΔP^l	Generation outage (MW)
η^{char}	Charging efficiency of ev battery
$\gamma_{b,m}$	Admittance of line between nodes b and m
λ_{ev}^{char}	Charging rate of ev (KW/h)
$\overline{f}^{nad}$	Maximum permissible under frequency (Hz)
$\overline{IL_t}$	IL load limit at time t
a_i, b_i, c_i	Conventional unit cost coefficients
$C_{s/w}^{curl}$	Renewable curtailment cost ($/MW)
C^{G2PL}	Cost of G2PL services ($/MWh)
C^{ls}	lost load cost ($/MWh)
$C_{i/pl}^{pfr/ffr}$	PFR/FFR cost from unit/PL
C^{rns}	Reserve not served
$C_i^{su/sd}$	Cost start-up/shut down of unit i ($)
f^{nl}	Nominal frequency (Hz)
H_i/H^l	Inertia constant for unit i/load l (s)
L^d	Load damping rate (1/Hz)
$l_{b,t}$	Load at bus b and time t (MW)
$P_{s,w,t}^{av}$	Available capacity of s/w units at time t (MW)
$P_{b,m}^{max}$	Maximum power transfer limit of line connecting buses b and m (MVA)
$P_i^{min/max}$	Minimum/maximum generation limit of unit i (MW)
P_t^{de}	Power demand for the time, t
R_i^{gov}	Governor ramp rate for unit i (MW/s)
RU_i/RD_i	Ramp up/down limit of unit i (MW/h)
$SOC_{ev}^{min/max}$	Minimum/maximum SOC limit on ev (KWh)
SUR_i/SDR_i	Startup/shutdown ramp of unit i (MW)

Abbreviation

DER	Distributed Energy Resources
DL	Deferrable Load
DR	Demand Response
ESS	Energy Storage Systems
EVs	Electric Vehicles
FFR	Fast Frequency Response
FL	Flexible Load
IL	Interruptible Load
PFR	Primary Frequency Response
PV	Photovoltaic
RES	Renewable Energy Sources
$RoCoF$	Rate of Change of Frequency
RTS	Reliability Test System
SFR	Secondary Frequency Response

carbon emission through electrification of transport sector. EVs can be considered as flexible load as EVs can be scheduled for their charging demand during their parking span in the parking lot. Furthermore, integration of EVs will also renders high penetration of RES by providing FFR [8]. The battery storage capacity of EVs makes it possible to provide FFR during contingency. In this context, smart flexible loads are a combination of interruptible loads (IL) and deferrable loads (DL) and power electronic interface. IL and DL are fast acting DR resources which can autonomously participate in DR and provide FFR [9]. IL can be disconnected during critical hours depending upon utility and consumer contracts for maintaining demand-generation balance. DL load can be shifted from peak load hours to off-peak load hours depending upon grid requirements [9].

IL curtails the peak demand. The duration of curtailment depends upon utility and consumer contract to balance generation and demand. DL can shift their time from peak demand to off-peak demand depending upon requirements. There are several well studied cases of IL and DL for frequency balancing services [10–12]. Demand side loads procured 1200 MW of frequency response in 2012 [12] and it was estimated that 30%–50% of grid balancing is delivered by demand side in 2020 [13]. A combination of smart flexible load and DERs is reported for providing fast PFR within 10 ac cycle is real time. Hence fast PFR can be achieved by optimal scheduling of available DERs and smart flexible loads [1]. A noteworthy feature of smart flexible loads and DER is that their energy consumption can be controlled and coordinated to create virtual storage. The coordination of DER and smart flexible load

Table 1
Comparison of proposed stochastic scheduling model for FFR with existing models.

Aspect	Deterministic models	Heuristic models	Proposed stochastic scheduling	Ref.
Handling uncertainty	Assumes fixed conditions, suboptimal outcomes	Ignores real-time uncertainties, non-optimal decisions	Incorporates uncertainties, enhancing robustness.	[25,26]
Adaptability	Not suitable for dynamic changes	Lacks flexibility to respond dynamically	Dynamically adjusts to real-time fluctuations	[27,28]
Computational efficiency	High, may sacrifice solution quality	Computationally efficient; not optimal	computationally demanding; accurate	[25,29]
Performance under high RE	Inadequate response	Not optimal performance	Suitable; accounts for variability.	[30,31]
Optimization approach	Not suitable for uncertainty	Limiting optimization scope	Utilizes stochastic optimization	[26,32]
Scalability	Struggle to scale effectively	Degrade with increased uncertainty	Scales effectively across different grid sizes	[33,34]
Response to grid events	Inadequate	Not adapt optimally to unexpected events	Rapid response capabilities	[35,36]
FFR capability	Not suitable for dynamic response requirement	Lacks comprehensive adaptability	Offers robust FFR	[1,37]
Flexible load integration	Not included	Lacks systematic optimization	Efficiently incorporates flexible loads	[9,38]

as virtual storage can complement grid management services like FFR. IL are used to arrest the frequency response in [14]. EVs can also be considered as flexible load. Integration of EVs in the smart grid can be a potential solution to support many grid services management such as FFR, regulation and spinning reserve [15]. However, large deployment of EVs bring associated challenges and concerns of uncoordinated charging demand in grid. The current literature has several studies cases of frequency control from EVs [15,16]. EVs contribution for primary frequency response (PFR) through smart scheduling strategies using unit commitment is reported in [17–19]. EVs potential is explored as secondary frequency response (SFR) in [20]. Few studies considered FFR from EVs [21–23]. Study in [24] employed EVs fleet scheduling for provision of frequency response with enhance RES penetration. The viable solution offered by smart grid for energy sustainability are RES, smart flexible loads and EVs. However, uncertainty and variability associated with RES impose a number of system operational challenges. The reason is that real time demand and supply should be balanced to maintain reliability and security. Therefore, it is required to address the uncertainty characterization of RES and EVs for accuracy of dispatch decisions and delivery of synthetic inertia and FFR.

This article brings a new look to the existing literature in the following areas: (I) Uncertainty characterization of wind generation, photovoltaic generation, and load-demand and EV uncertainty. (II) Utilization of IL, DL, EVs to enhance grid resilience and support FFR. (III) A comprehensive stochastic scheduling framework that maps the frequency security parameters such as RoCoF and frequency deviation to support the FFR requirement and optimize the support from flexible loads.

Previous works in FFR scheduling primarily focused on deterministic approaches or heuristic-based models, which are often insufficient in handling the inherent uncertainties present in power systems, particularly those with significant RE penetration. The limitations of existing approaches are compared with the proposed FFR constrained stochastic scheduling framework as shown in Table 1. This table highlights the advantages of the proposed stochastic scheduling approach in terms of handling uncertainties, adaptability, and FFR performance in high renewable integration scenarios, making it a more robust solution for the modern power systems.

The scientific aim of the research is to lay groundwork to highlight the significance of coordination between DER and loads for reliable and secure systems. High penetration of DER such as RES and EVs is anticipated in the future grid. Hence there is a need for in-depth investigation of optimal coordination between DER and loads such as IL and DL. The subject of the research is to assess contribution EVs, IL and DL for FFR, their scheduling with high penetration of RES requires investigation.

In this context the contribution of this study is summarized as follows:

- To develop a stochastic scheduling framework for flexible loads, including EVs, interruptible loads ILs, and DLs, under high RES penetration to provide FFR services. The scheduling framework accounts for the uncertainties of RES and loads within a day-ahead planning context.
- To evaluate the techno-economic parameters of frequency security criteria, such as RoCoF and frequency deviation, at various levels of support from flexible loads, RES curtailment, FFR cost, and operation cost.

The rest of the paper is organized as follows: Section 2 discusses problem overview and formulation. Section 3 provides simulation results of case study. Finally, in Section 4 conclusion of paper is presented.

2. Problem formulation

Due to the intermittent and uncertain nature of RES, maintaining system reliability and security is a challenging task for operators. This challenge becomes even more pronounced during contingencies such as generator outages, which require an adequate frequency response to secure post-fault frequency dynamics. FFR can be provided by smart, flexible loads, including EVs, which are capable of delivering a rapid response through optimal scheduling. Fig. 1 details out the various aspects included in the problem formulation.

It is important to note that the intermittent and uncertain behavior of RES affects the dispatch of conventional generating units, which in turn impacts overall system operation [39,40]. This section focuses on FFR-constrained scheduling involving RES, IL, DL, and EVs. Additionally, it discusses the uncertainty characteristics associated with load and RES.

2.1. Fast frequency response

FFR involves the rapid delivery of power from a service provider, typically within 2 s following a contingency, to mitigate the RoCoF

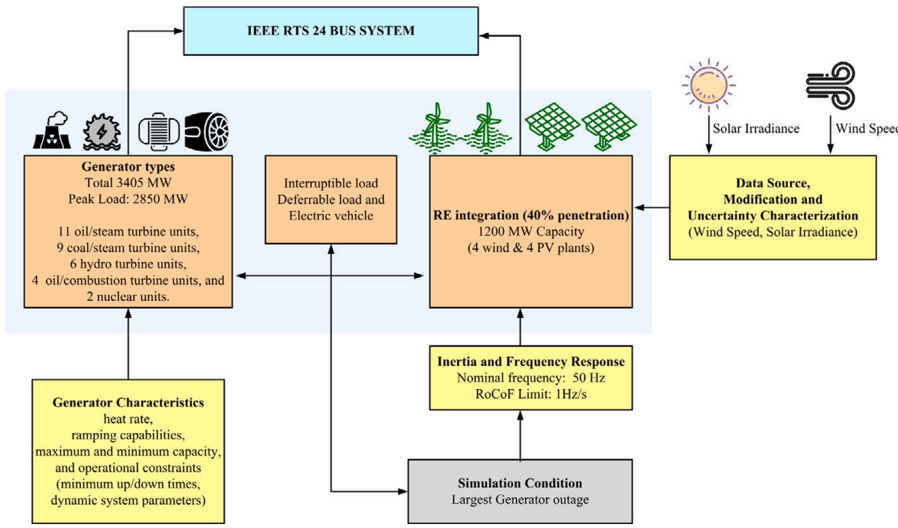

Fig. 1. Problem overview.

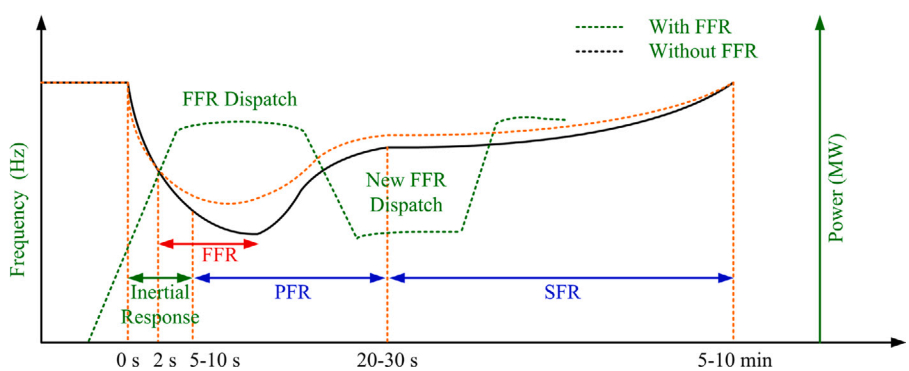

Fig. 2. Frequency generator characteristics following a generator outage [2].

and maintain this response for approximately 10 seconds [2,41]. This service complements Primary Frequency Response (PFR), providing additional time for the system to stabilize and maintain frequency levels above the threshold for Under Frequency Load Shedding (UFLS). Consequently, the coordination between FFR and PFR helps stabilize frequency deviations after a fault. As shown in Fig. 2, the impact of FFR on improving post-fault frequency characteristics is evident following a generator outage event.

The interaction of the electrical power (ΔP_e) and the mechanical power (ΔP_m) applied to the rotor of a conventional generator because of the frequency variation is captured by the well-known swing equation present in Eq. (1). Here, H_{sys} denotes the system inertia constant measured in seconds, and $\frac{\mathrm{d}\Delta f}{\mathrm{dt}}$ is the rate of change of frequency also known as RoCoF.

$$2H_{sys}\frac{d\Delta f}{dt} = \Delta P_m - \Delta P_e \tag{1}$$

The FFR is required in the system during event of contingency. During contingency RoCoF increases rapidly which may results in operation of frequency sensitive relays and blackout in worst cases. FFR acts by supplying electrical power in controlled mode to partially balance power imbalances (ΔP^l). This leads to reduction of (ΔP^l) to ($\Delta P^{l'}$)). The reduction in (ΔP^l) is shown in Eqs. (2)–(3). Here, P_x^{ffr} represents FFR support from fast acting resources like EVs.

$$\Delta P^l = \Delta P_m - \Delta P_e \tag{2}$$

$$\Delta P^{l'} = \Delta P^l - P_x^{ffr} \tag{3}$$

2.2. Uncertainty characterization

This section discusses the depiction of uncertainties in load demand, wind power, PV generation, and EVs. These uncertainties are typically modeled using probability density functions (PDFs), which provide a reliable method for characterizing uncertainty. However, while PDFs are effective for this purpose, they can significantly complicate the computational feasibility of the problem formulation [42].

To address the uncertainty characterization issue, a scenario-based methodology is employed in this work [23,25,31]. Instead of relying solely on PDFs, this approach involves generating a large number of potential scenarios that capture the various possibilities associated with the uncertainties. These scenarios represent different possible states of the system under varying conditions.

Once a comprehensive set of scenarios is generated, a scenario reduction algorithm is applied to condense this large set into a manageable number of uncertainty realizations. This reduction process ensures that the key characteristics and variability of the original uncertainties are preserved, while also improving the computational efficiency of the subsequent analysis and decision-making processes.

2.2.1. Wind generation uncertainty

The power generation from wind is primarily influenced by wind speed and the characteristics of the wind turbine. However, wind speed is inherently intermittent and unpredictable, making it necessary to model this variability accurately. In this context, the Rayleigh PDF is often employed to represent the statistical distribution of wind speed [43].

In this work, the wind speed at each time step t, denoted as $f_r^t(v)$, is generated using the Rayleigh PDF. The Rayleigh distribution is particularly suited for modeling wind speed because it effectively captures the typical behavior of wind patterns, where lower speeds are more frequent, and the likelihood of very high or very low speeds decreases.

By using this statistical approach, the generated wind speed data can more realistically reflect the intermittent nature of wind, allowing for more accurate simulations and assessments of wind power generation over time. The specific mathematical expression used to generate wind speed from the Rayleigh PDF is provided in the following equation:

$$f_R^t(v) = \left(\frac{2v}{c^2}\right) exp\left[-\frac{v^2}{c}\right] \tag{4}$$

where f_R^t is Rayleigh function in which v is the wind speed at time t and c represents the Rayleigh scale parameter. The power obtained from wind speed for each time interval t can be estimated as follows [44]:

$$P_{wt}^t = \begin{cases} 0 \le v_t < v_{ci} & \\ P_{rated} \times \frac{v_t - v_{ci}}{v_r - v_{ci}} & v_{ci} \le v_t < v_r \\ P_{rated} & v_r \le v_t \le v_{co} \\ 0 & v_t \geqslant v_{co} \end{cases} \quad \forall t \in T \tag{5}$$

where P_{wt}^t is wind power at time t, v_{ci}, v_{co}, v_r respectively denotes cut in, cut-off and rated speed of wind turbine. P_{rated} represents the rated power of wind turbine.

2.2.2. Solar photovoltaic (PV) generation uncertainty

The power generated from solar photovoltaic (PV) depends upon factors such as solar irradiance, tilt angle, module area. The power generation mainly depends upon solar irradiance assuming other factors constant. solar irradiance is modeled using Rayleigh PDF. Therefore, power generation from PV can be expressed as:

$$P_{pv} = f(s_{pv}) \tag{6}$$

The power generation from PV can be evaluated as:

$$P_{pv,t} = \begin{cases} P_{pv,r} & s_{pv,t} > s_{pv,r} \\ (\frac{s_{pv,t}}{s_{pv,r}}) \times P_{pv,r} & s_{pv,t} < s_{pv,r} \end{cases} \quad \forall t \in T \tag{7}$$

where, $P_{pv,t}$ is power generated from solar at time t, $s_{pv,t}$, $s_{pv,r}$, and $P_{pv,r}$ is actual solar irradiance, rated solar irradiance, and rated power from PV respectively.

2.2.3. Load demand uncertainty

In this work, the associated uncertainty with load demand is modeled using a normalized PDF. The normalized PDF can be expressed as:

$$f_N^t(l) = \frac{1}{\sigma\sqrt{2\pi}} \times exp\left[-\left(\frac{l - \mu_l}{2\sigma_l^2}\right)\right] \tag{8}$$

where, $f_N^t(l)$ is the normal pdf of load demand; l is load demand at time t; μ_l represents the mean of load demand and σ_l indicated the standard deviation of load demand.

2.2.4. EVs uncertainty

The uncertainty in EVs demand arises from the driving pattern. These uncertain parameters can be (i) arrival time (ii) departure time (iii) driven distance (iv) battery capacity of connected EVs (v) charging and discharging efficiency (vi) initial state of energy (SOE) of EV. These parameter depends on EVs owner preference and hence are extremely uncertain. In order to account for EVs uncertainty and mimic realistic scenarios for evaluating scheduling, the parameters are generated from PDF described as follows [45]:

$$f_N^t(T_{ar}) = \frac{1}{\sigma\sqrt{2\pi}} \times exp\left[-\left(\frac{T_{ar} - \mu_{T_{ar}}}{2\sigma_{T_{ar}}^2}\right)\right] \tag{9}$$

$$f_N^t(T_{dr}) = \frac{1}{\sigma\sqrt{2\pi}} \times exp\left[-\left(\frac{T_{dr} - \mu_{T_{dr}}}{2\sigma_{T_{dr}}^2}\right)\right] \tag{10}$$

where, $f_N^t(T_{ar})$ and $f_N^t(T_{dr})$ is normal pdf for arrival and departure time respectively, $\mu_{T_{ar}}, \sigma_{T_{ar}}$, $\mu_{T_{dr}}$, $\sigma_{T_{dr}}$ mean and deviation of arrival and departure time respectively. The initial SOC is estimated using distance driven (D_n) and all electric range (AER_n) of n_{th} EV. The depth of discharge is not more than 80% to reduce the degradation of battery. Therefore, initial SOC_n of n_{th} EV can be defined as:

$$SOC_n^{ini} = 1 - \frac{D_n}{AER_n} \tag{11}$$

The uncertainty associated with distance traveled can be described using as a lognormal pdf as follows:

$$f_{LN}(D_{trav}) = \frac{1}{D_n\sqrt{2\pi(\sigma_n)^2}} \times exp\left[\frac{-(lnD_n - \mu_n)^2}{2(\sigma_n)^2}\right] \tag{12}$$

where μ_n and σ_n is the mean and standard deviation of distance traveled by n_{th} EV.

2.3. Scenario generation and reduction

In this work, a large number of scenarios are generated to approximate the Probability Density Function (PDF) of uncertain parameters. Generating a substantial number of scenarios enhances the accuracy of the stochastic evaluation, as it allows for a more detailed representation of the underlying uncertainties. However, this approach also comes with a drawback: the increased number of scenarios can significantly reduce the computational efficiency of the problem.

To address this issue, it is essential to determine a finite set of scenarios that balance the need for accuracy with computational feasibility. The process of scenario generation and reduction, aimed at approximating the PDF, is outlined in the following algorithm:

Step 1: Scenario Generation
Initially, a large number of scenarios are generated based on the PDF for each uncertain parameter, such as wind speed, solar PV output, load demand, and electric vehicle (EV) behaviors. For each parameter, a total of $\overline{S}$ scenarios are created. Each scenario $\overline{s}$ in the set $\overline{S}$ represents a specific combination of conditions, including load demand, wind speed, EV arrival and departure times, and distances traveled for each time interval. This comprehensive set of scenarios aims to capture the full range of possible outcomes for these uncertain variables.
Step 2: Scenario Reduction
In this step, the large set of scenarios generated in Step 1 is reduced using a backward reduction technique, as described in [46, 47]. The goal of this technique is to condense the number of scenarios to a more manageable and computationally efficient set, denoted by N_s. This reduced set still accurately represents the original range of uncertainties while being more practical for computational analysis. The method outlined in [46] is particularly useful for validating that the reduced set of scenarios maintains the integrity and representativeness of the initial, larger set.
Through this process, the reduced number of scenarios N_s can be used to evaluate the solution within the limits of computational feasibility, ensuring that the stochastic model remains both accurate and efficient.

2.4. Frequency security constrained scheduling framework

The scheduling framework developed in this work is frequency constrained SCUC model to balance system demand, reserve and FFR requirement with high penetration of RES. The simulations are performed on General Algebraic modeling System (GAMS) software using

CPLEX solver. Stochastic scheduling framework is modeled to incorporate probabilistic scenarios, FFR constraints, FL constraints to map the post fault frequency dynamics and uphold the frequency security criteria like RoCoF and frequency deviation. Probabilistic scenarios are used to model various uncertainties.

The conventional units, EVs, IL, DL and RES are scheduled to fulfill demand of grid and FFR requirements. The aim of the stochastic SCUC scheduling formulation is to minimize system operation cost. The input to stochastic SCUC are parameters of conventional generators and EVs, uncertainty of RES and cost components of ancillary and service components. Eq. (13) elaborates the expression of proposed scheduling framework.

$$\sum_{\omega} \Pi_{\omega} \sum_{t} \Bigg(\sum_{i} \big(a_i P_{i,t,\omega}^2 + b_i P_{i,t,\omega} + c_i + C_i^{su}.\beta_{i,t,\omega} + C_i^{sd}.\gamma_{i,t,\omega} + P_{i,t,\omega}^{pfr}.C_i^{pfr} \big) + (IL_{i,t} + DL_{i,t}).C^{DR} + \sum_{b} LS_{b,t,\omega}.C^{ls} + P_{t,\omega}^{rns}.C^{rns} + \sum_{s/\omega} P_{s/w,t,\omega}^{curl}.C_{s/w}^{curl} + \sum_{pl} \big(P_{pl,t,\omega}^{G2PL}.C^{G2PL} + P_{pl,t,\omega}^{ffr}.C_{pl}^{ffr} \big) \Bigg) \tag{13}$$

In the Eq. (13) first part denotes operating cost of conventional unit, cost of start up and shut down cost, PFR support from conventional units and cost of IL and DL. Second and third part represents penalty cost for load shedding and reserve not served respectively. The penalty for curtailment of RES (PV and wind) is expressed in fourth part. Last part denotes the participation cost of EVs as aggregated load and FFR support.

2.4.1. Traditional generation unit operational constraints

The traditional generation unit system operation constraints of are considered using Eqs. (4)–(12). The additional constraints for conventional units are expressed in Eqs. (14)–(18). Eq. (14) discusses maximum rated capacity of unit, limited by their response provision. Frequency response requirements are determined on the basis of post fault dynamic frequency evolution. The assumption for reserve requirement is 50% of largest generator capacity. The ramp up and ramp down constraints are expressed in Eqs. (15)–(16). Power balance equations are modeled using Eqs. (17)–(18).

$$P_i^{min} \le P_{i,t,\omega} + P_{i,t,\omega}^{res} + P_{i,t,\omega}^{pfr} \le P_i^{max} \quad \forall i,t,\omega \tag{14}$$

$$P_{i,t,\omega} - P_{i,t-1,\omega} + P_{i,t,\omega}^{res} + P_{i,t,\omega}^{pfr} \le RU_i.\alpha_{i,t,\omega} + SUR_i.\beta_{i,t,\omega} \quad \forall i,t,\omega \tag{15}$$

$$P_{i,t,\omega} - P_{i,t-1,\omega} + P_{i,t,\omega}^{res} + P_{i,t,\omega}^{pfr} \le RD_i.\alpha_{i,t,\omega} + SUR_i.\beta_{i,t,\omega} \quad \forall i,t,\omega \tag{16}$$

$$P_{bm,t,\omega} = \gamma_{bm} \big(\theta_{b,t,\omega} - \theta_{m,t,\omega} \big) S_b \quad \forall t,\omega \tag{17}$$

$$-P_{max}^{bm} \le P_{bm,t,\omega} \le P_{max}^{bm} \forall t,\omega \tag{18}$$

2.4.2. Flexible load operational constraints

1. The operational constraint with flexible loads: IL requirement for each hour is shown by the Eq. (19).

$$IL_t = P_t^{de} = P_t^{de} - \left(\sum_{t=1}^{T} \sum_{i=1}^{NT} y_{i,t}.p_{i,t} + pv_t^{avl} \right) \quad \forall t \in T \quad i \in NT \tag{19}$$

Required IL capacity is calculated for each hour.
Subject to:

$$0 \le IL_t \le \overline{IL_t} \tag{20}$$

$$IL_t \le \overline{IL_t} \tag{21}$$

Constraint (20) determine the minimum and maximum limit of the IL . Required IL limit should always less than maximum limit of IL is shown by constraint (21).

2. IL contracts constraint: IL formulation has few contracts between customer and ISO. These contracts are followed as: (i) Maximum hour of curtailment for a day

$$IL_h^{max} = \sum_{t=1}^{T} uIL \tag{22}$$

$$IL^{max} = IL_t^{fix} \tag{23}$$

Constraint (22) shows the total hours in which IL participated and maximum hours of curtailment is already fixed (15 h for a day) by agreement as shown by constraint (23).
Subject to:

$$IL_t \le P_t^{de} \tag{24}$$

$$IL_t \le M * uIL \tag{25}$$

where, M is a large positive variable.
(ii) Maximum load curtailment for a day

$$IL_t \le \overline{IL_t} \tag{26}$$

Constraint (26) shows that maximum load curtailment should always less than equal to the maximum capacity of IL load.

2.4.3. Operational constraint of EVs

EV scheduling is managed by EV Aggregators (EVA), entities that serve as intermediaries between EV owners and system operators. The primary role of the EVA is to coordinate the charging of EVs in PLs while considering the interests of the owners. The scheduling strategy adopted by the EVA aims to optimize the charging of EVs to enhance grid operations by providing ancillary services, such as FFR.

In this context, EVs charge under the Grid-to-Vehicle (G2V) mode, where their rapid response capabilities make them a promising technology for supporting grid services like FFR. Power is exchanged between EVs parked in PLs during office hours and the grid through the Parking Lot-to-Grid (PL2G) mode. The charging power required by EVs in PLs is estimated based on parameters such as arrival time, departure time, distance traveled, and initial State of Charge (SOC). These parameters are modeled using Eqs. (9) to (12).

The charging process of EVs and the associated constraints are modeled using Eqs. (27) to (38). The number of EVs available in PLs is determined based on the arrival and departure times of EVs, as described in Eqs. (27) to (29). The total available State of Energy (SOE) based on the EVs parked at time t is expressed in Eqs. (30) to (34). The expected SOC of EVs, considering the distance traveled, is estimated using Eqs. (32) and (33), where En_{ev}^{trav} represents the energy required for driving, D^{trav} is the distance traveled, and E^{cons} is the per-kilometer energy consumption of the EV.

The charging rate of EVs is defined by Eq. (35), and the SOE at each time interval is evaluated using Eq. (36). The permissible SOC limits are provided in Eq. (37). Finally, the FFR capacity from aggregated EVs at time t is given in Eq. (38).

$$N_{pl,b,t,\omega}^{arv} = \sum_{t \in t^{arv}} \sum_{ev} N_{ev,b,t,\omega} \quad \forall b \tag{27}$$

$$N_{pl,b,t,\omega}^{dep} = \sum_{t \in t^{dep}} \sum_{ev} N_{ev,b,t,\omega} \quad \forall b \tag{28}$$

$$N_{pl,b,t,\omega}^{net} = N_{ev,b,t-1,\omega} + N_{ev,b,t,\omega}^{arv} - N_{ev,t,\omega}^{dep} \tag{29}$$

$$SOE_{pl,b,t,\omega}^{arv} = \sum_{t \in t^{arv}} \sum_{ev} SOC_{ev,b,t,\omega}^{ini} R_{ev} \tag{30}$$

$$SOE_{pl,b,t,\omega}^{dep} = \sum_{t \in t^{exp}} \sum_{ev} SOC_{ev,b,t,\omega}^{exp} R_{ev} \tag{31}$$

$$En_{ev}^{trav} = D^{trav} En^{cons} \tag{32}$$

$$SOC_{ev,b,t,\omega}^{exp} = SOC_{ev}^{max}.20\% + \frac{En_{ev}^{trav}}{R_{ev}} \tag{33}$$

$$SOC^{net}_{pl,b,t,\omega} = SOC^{net}_{pl,b,t-1,\omega} + SOE^{arv}_{pl,b,t,\omega} - SOE^{dep}_{pl,b,t,\omega} \tag{34}$$

$$P^{G2PL} \leq \chi^{char}_{ev,t}.N^{net}_{pl,b,t,\omega}.\lambda^{char}_{ev} \tag{35}$$

$$SOE^{agg}_{pl,b,t,\omega} = SOE^{agg}_{pl,b,t-1,\omega} + SOE^{arv}_{pl,b,t,\omega} + P^{G2PL}_{pl,b,t,\omega}.\eta^{char} \tag{36}$$

$$SOC^{min}_{ev} \leq SOC_{ev,b,t,\omega} \leq SOC^{max}_{ev} \tag{37}$$

$$P^{ffr}_{pl,t,\omega} = \sum_b \left(PL^{ini}_{pl,b,t,\omega} - P^{G2PL}_{pl,b,t,\omega} \right) \tag{38}$$

2.4.4. Post fault system frequency requirements

The frequency response requirements during a contingency event are modeled using a steady-state, day-ahead stochastic Security-Constrained Unit Commitment (SCUC) model. This model ensures that FFR is available during real-time contingencies by scheduling fast-acting units in advance, during the day-ahead planning phase.

The equations from Eq. (39) to Eq. (45) detail the modeling of system inertia, Rate of Change of Frequency (RoCoF), frequency nadir, and steady-state frequency:

System Inertia (Eq. (39)): This equation represents the system inertia, which includes the rotational inertia of generator rotors and load machines.

RoCoF After Fault (Eqs. (40)–(41)): These equations model the RoCoF following a fault, which is primarily influenced by system inertia, the lost generation capacity, and the FFR response from electric vehicles (EVs).

Frequency Nadir and Nadir Time (Eqs. (42)–(43)): These equations describe the frequency nadir (the lowest frequency reached after a disturbance) and the time at which it occurs, taking into account factors such as lost capacity, ramp rates, and dead bands.

Primary Frequency Response (PFR) and Quasi-Steady-State Frequency (Eq. (44)): PFR is responsible for stabilizing the frequency at a quasi-steady state after the initial disturbance.

Compensation for Lost Generation (Eq. (45)): This equation addresses the compensation for lost generation based on the response time of the PFR, ensuring the system's frequency is stabilized after the initial drop.

Together, these equations provide a comprehensive framework for modeling the system's frequency response to contingencies, from initial inertia to real-time frequency stabilization.

$$SI_{t,\omega} = \frac{P^{max}_{i,t,\omega} H_i u_{i,t,\omega} + H^l L_{t,\omega}}{f^n} \tag{39}$$

$$RoCoF_{t,\omega} = \frac{\Delta P^{l'}_{t,\omega}}{2SI_{t,\omega}} \leq \overline{RoCoF} \quad \forall t,\omega \tag{40}$$

$$\Delta P^{l'}_{t,\omega} = \Delta P^l - \sum_{pl} P^{ffr}_{pl,t,\omega} \quad \forall t,\omega \tag{41}$$

$$f^{nad}_{t,\omega} = f^{nl} - \Delta f^{db} - \frac{f^{nl}(\Delta P^{l\varepsilon}_{t,\omega})^2}{4\sum_i P^{max}_{i,t,\omega}.H_i U_{i,t,\omega} R^{gov}_i} \leq \overline{f}^{nad} \tag{42}$$

$$t^{nad}_{t,\omega} = \frac{4SI_{t,\omega}(f^0 - \Delta f^{db} - f^{ulfs}) + 2SI_{t,\omega}\Delta f^{db}}{\Delta P^{l\varepsilon}} \tag{43}$$

$$\Delta f^{ss}_{t,\omega} = \frac{\Delta P^{l\varepsilon}}{D.L^d_f} \leq \Delta \overline{f}^{SS} \tag{44}$$

$$\Delta P^{l\varepsilon}_{t,\omega} = \Delta P^{l'} - \sum_i P^{ffr}_{i,t,\omega} \quad \forall t,\omega \tag{45}$$

2.4.5. Renewable generation and power balance constraints

The RES generation and curtailment is modeled in Eqs. (46)–(47).

$$P^{gen}_{w,t,\omega} + P^{curl}_{w,t,\omega} \leq P^{av}_{w,t,\omega} \tag{46}$$

$$P^{gen}_{s,t,\omega} + P^{curl}_{s,t,\omega} \leq P^{av}_{w,t,\omega} \tag{47}$$

The power balance constraints are governed by generation from conventional units, load shedding, charging/discharging of aggregated EVs and net load demand respecting line limits. Eq. (48) give the balance constraint and Eq. (49) give net load in the grid.

$$\sum_i P_{i,b,t,\omega} + LS_{b,t,\omega} - l^{net}_{b,t,\omega} - \sum_{pl} P^{G2PL}_{pl,b,t,\omega} = P_{bm,t,\omega} \quad \forall b,t,\omega \tag{48}$$

$$l^{net}_{b,t,\omega} = l_{b,t,\omega} - \sum_s P_{s,t,\omega} + \sum_w P_{w,t,\omega} \quad \forall b,t,\omega \tag{49}$$

3. Case study

The IEEE Reliability Test System (RTS) for a single area was employed to validate the proposed day-ahead mixed integer stochastic scheduling model. This system includes 24 buses, with 17 load buses and 32 generators, featuring a total installed capacity of 3405 MW and a peak load of 2850 MW. The generation mix comprises eleven oil/steam turbine units, nine coal/steam turbine units, six hydro turbine units, four oil/combustion turbine units, and two nuclear units. Key generator characteristics, such as heat rate, ramping capabilities, maximum and minimum capacity, and operational constraints (minimum up/down times, dynamic system parameters), were incorporated into the model [48].

The RE plants, including wind farms and PV plants, were mapped respecting the line transfer capacities of the RTS network. The study was conducted across various RE integration levels, ranging from 10% to 40% of the total generation, in 10% increments. A steady-state model was used in the proposed scheduling model to ensure adequate frequency response during contingencies by scheduling sufficient units in the day-ahead market.

Four wind farms and four PV plants, with a total generation capacity of 1200 MW (representing 40% penetration), were integrated into the system. Historical hourly time series data for solar irradiance and wind speed was obtained from system-specific coordinates, and power was calculated for PV generation and for wind power [23,34]. The data used spanned from January 1, 2020, to December 31, 2020, with wind speed data sourced from the Illinois Institute of Rural Affairs, USA, and PV irradiation data from Chicago, USA.

Wind farms were strategically placed based on the transmission line lengths, ensuring that their locations did not exceed line transfer capacities. VESTAS V90 turbines were chosen for the wind units, and technical details regarding these turbines were obtained from the manufacturer database. The wind speed was modeled using the Weibull distribution, while solar irradiance was modeled using the Normal distribution. The standard deviation of these resources followed a half-normal distribution to account for natural variability [36].

In real-world power systems, an emergency power supply is essential for handling sudden grid events and maintaining critical system parameters. In this work, the IEEE RTS system is modified to include a 10% headroom capacity for addressing emergency grid imbalances. Flexible generator units, such as U197 and U350, are employed to provide a quick response for emergency power supply. Additionally, the energy storage capability of EVs serves as a crucial emergency power source during worst-case contingencies.

At this stage, wind and photovoltaic (PV) penetration levels are incrementally increased, and the net load is calculated for each penetration level, as illustrated in Fig. 3.

3.1. FFR performance with various level of flexible loads

Flexible load participation in FFR significantly impacts the RoCoF and frequency deviation limits. It is observed that increasing the penetration level of flexible loads from 0% to 40% reduces the overall net load. Consequently, commitment decisions are altered due to the decreasing net load, which results in reduced overall inertia. This reduction in inertia leads to an increase in RoCoF and frequency

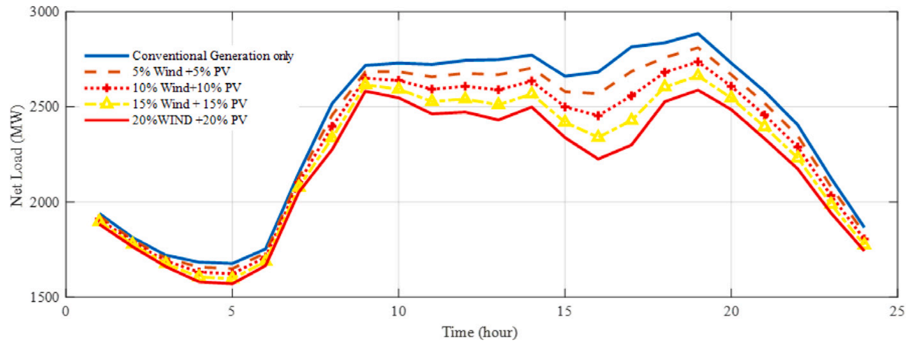

Fig. 3. Netload with varying wind and PV penetration.

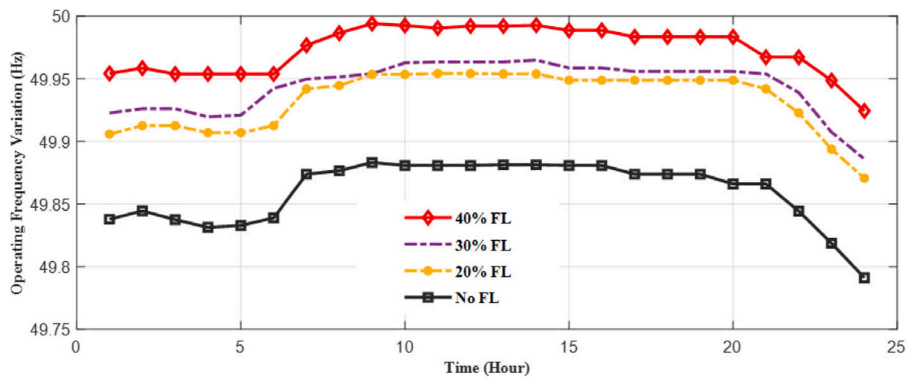

Fig. 4. Frequency deviation response with variation in flexible load support.

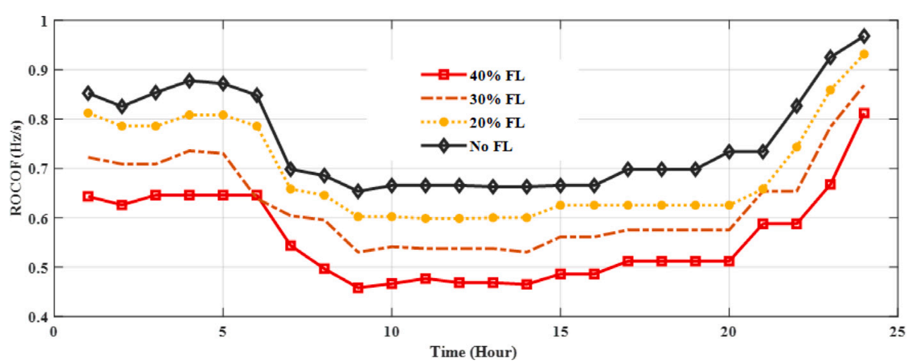

Fig. 5. RoCoF with variation in flexible load support.

deviation, as illustrated in Figs. 4 and 5. Notably, when penetration exceeds 30%, the RoCoF variation becomes more pronounced, nearing the prescribed frequency security limit of 1 Hz/s in Hour 24 before approaching the frequency deviation threshold. This heightened RoCoF could trigger RoCoF relays and high variation in frequency deviation, potentially leading to the curtailment of RES. Fig. 6 depicts the high frequency deviation causes significant RES curtailment, and increased cost for system operation. Frequency deviation below 49.8 Hz cause more than 30% RES curtailment. This indicates the increased requirement for flexible load support for FFR as depicted in Figs. 4, 5. Hence, flexible load levels assist to maintain grid stability and avoid frequency security limit breaches.

3.2. FFR adequacy with system frequency deviation

In this section, we estimate the available Fast Frequency Response (FFR) and its requirement for the largest infeed loss, which is 400 MW. Analysis indicates that the frequency nadir for the studied system is 49.65 Hz. To quickly correct the generation-demand imbalance, approximately 600 MW of FFR is necessary. The case study reveals that the system has sufficient FFR under all conditions to keep the frequency above the minimum threshold. Consequently, there is no need for additional FFR under the given circumstances. However, it is important to note that the FFR requirement increases when the frequency nadir is lower, as illustrated in Fig. 7

This means that while the current FFR is adequate to handle a 400 MW loss without dropping below the critical frequency limit, a more substantial frequency drop would necessitate a higher amount of FFR to stabilize the system. Thus, ensuring the availability of sufficient FFR is crucial for maintaining system stability and preventing frequency from falling to dangerously low levels during significant infeed losses.

3.3. FFR from ILs, DLs and EVs

Fig. 8 and Table 2 illustrates the contributions of various flexible loads – IL, DL, and EVs – to FFR over a day-ahead system operation.

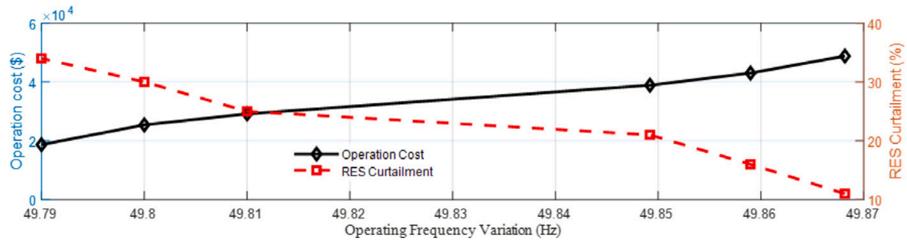

Fig. 6. RES curtailment and operation cost with operating frequency variation.

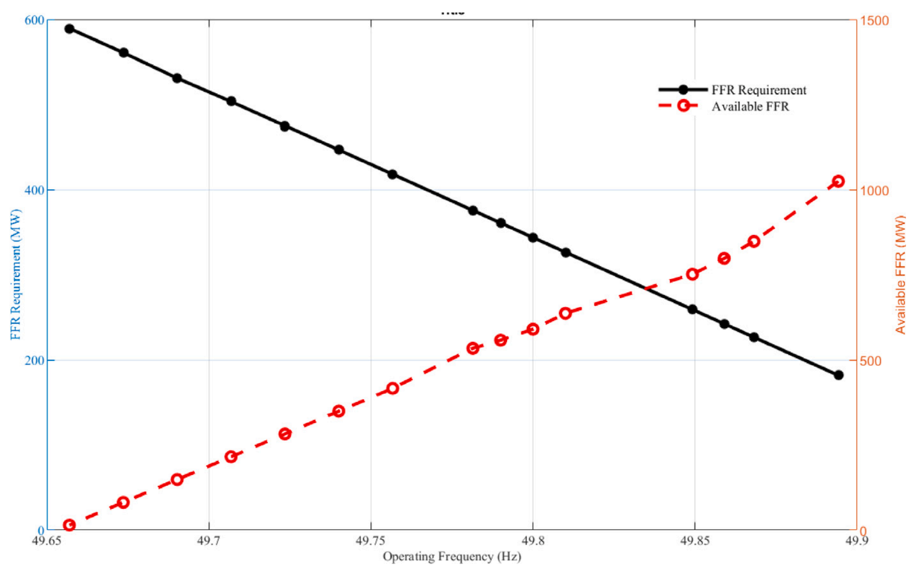

Fig. 7. FFR requirement with frequency deviation.

These flexible loads play a critical role in stabilizing grid frequency by providing rapid adjustments to demand. ILs, which can be quickly reduced or disconnected, offer immediate relief to the grid, while DLs, whose consumption can be shifted in time, provide additional flexibility in managing frequency deviations. EVs, with their potential for both charging and discharging, contribute dynamically to the grid's frequency stability. It is observed from the figure that the combined contributions of IL, DL, and EVs, along with their individual responses, are maximized when the RoCoF and frequency deviation are at their highest.

Table 2 highlights the FFR contributions from IL, DL and EVs. The table outlines the contributions to FFR from three sources: IL, DL, and EV. The IL contribution ranges from 146 MW to 280 MW, demonstrating that it plays the most significant role in providing FFR throughout the 24-h period. The highest IL contribution occurs during the 11th hour (280 MW), while the lowest is observed in the 24th hour (146 MW). This suggests that IL has a substantial and relatively stable share of FFR provision, with minor fluctuations over the course of the day.

The DL contribution varies from 10 MW to 40 MW, indicating a moderate but essential role in supporting FFR. The peak contribution from DL occurs in the 9th hour (40 MW), while the minimum is noted in the 2nd, 3rd, and 14th hour (10 MW). The variations in DL contributions highlight its potential to supplement the FFR from IL, especially during peak demand periods.

The EV contribution ranges between 5 MW and 18 MW, the lowest among the three sources. The highest EV contribution is recorded in the 5th hour (18 MW), while the lowest occurs in the 12th and 13th hours (5 MW). This indicates that while EVs have a relatively smaller share in the total FFR provision, their contribution can still be valuable, particularly when combined with other sources to enhance system flexibility and stability.

Together, these flexible resources enhance the grid's ability to respond to fluctuations in supply and demand, thereby supporting the system's overall reliability and security.

3.4. Cost analysis

The Fig. 9 illustrates the variation in operation cost and Fast Frequency Response (FFR) cost with increasing contributions from flexible loads and higher penetration of Renewable Energy Sources (RES). As RES penetration increases, the overall operation cost decreases due to the reduced reliance on conventional units, which results in fewer of these units being committed online per hour. However, there is a marginal increase in FFR costs, which only adds about 0.3% to the total operation cost. This slight increase is attributed to the provision of FFR, as the cost of synchronous inertia is considered negligible for the scheduling horizon, given the system's sufficient inertia and Primary Frequency Response (PFR).

Additionally, the study reveals that a decrease in the RoCoF from 1 Hz/s to 0.4 Hz/s leads to an 18% increase in operation costs and a 20% increase in RES curtailment. Similarly, a frequency deviation from 49.87 Hz to 49.79 Hz results in increased RES curtailment but a 16% reduction in operation costs. This reduction in costs is due to the combined effect of fewer committed conventional generators and increased contributions from flexible loads. These findings are crucial for establishing system frequency security parameters, such as RoCoF settings and FFR requirements, especially in low-inertia power systems. Understanding these dynamics will help in optimizing both cost and reliability in future grid operations.

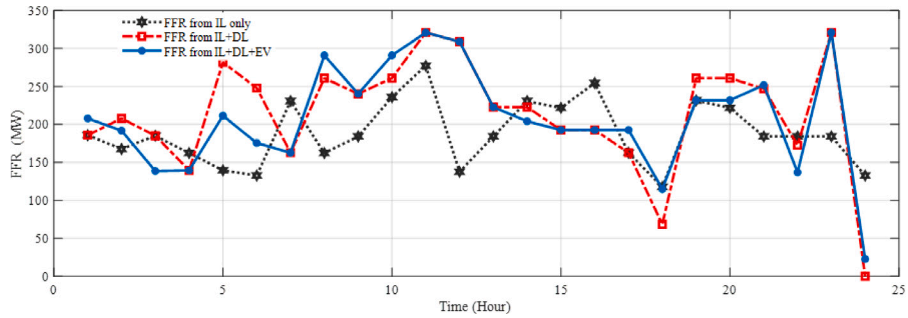

Fig. 8. FFR contribution from IL, DL and EV flexible loads.

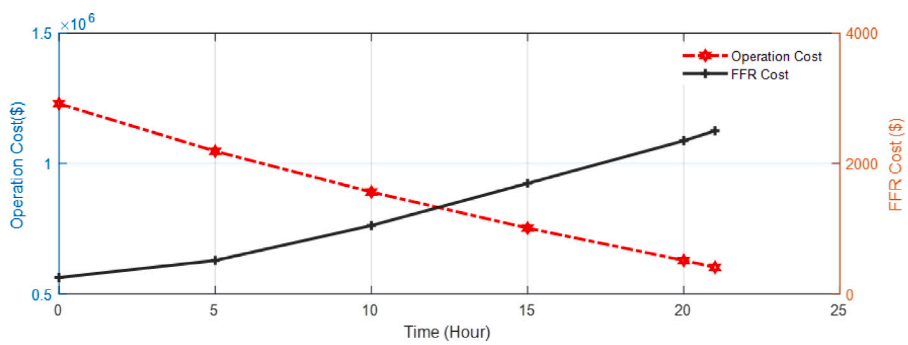

Fig. 9. FFR cost and operation cost variation.

Table 2
FFR contributions from IL, DL, and EV over 24 h.

Hour	IL contribution (MW)	DL contribution (MW)	EV contribution (MW)
1	185	17	8
2	202	10	7
3	222	10	7
4	162	25	12
5	194	34	18
6	255	17	8
7	226	27	12
8	176	28	10
9	190	40	10
10	210	30	12
11	280	20	10
12	270	20	5
13	240	20	5
14	220	10	5
15	190	20	10
16	180	20	13
17	210	20	10
18	220	17	10
19	245	17	12
20	257	17	10
21	220	20	12
22	210	20	12
23	226	27	12
24	146	36	16

The quantitative analysis reveals that incorporating FFR constraints into the stochastic scheduling framework offers significant advantages. As operating frequency increases from 49.79 Hz to 49.87 Hz, the operational cost rises by approximately 87%, from 2.1×10^4 dollars to 4.6×10^4 dollars. This cost increase is a result of stricter frequency control requirements. Simultaneously, RES curtailment drops by 57%, from around 35% to 15%, indicating that the system can integrate more renewable energy with less need for curtailment. The reduction in curtailment is achieved due to the FFR support provided by flexible resources that help to stabilize frequency without resorting to conventional generation methods. Thus, the quantitative analysis demonstrates that the trade-off between increased operational cost and decreased RES curtailment favors the inclusion of FFR, enabling more efficient renewable energy integration while maintaining grid stability.

The proposed framework is flexible and scalable, and with the appropriate adjustments, it can be applied to various power networks, whether larger, isolated, or feature different generation mixes. The key to its adaptability lies in recalibrating system-specific parameters and transmission constraints. Further work might involve case studies on larger, more complex systems to validate the framework's scalability and robustness.

3.5. Computational performance

The proposed stochastic scheduling framework, which includes FFR constraints and accounts for wind and PV penetration alongside FL constraints, requires approximately 1.5 times more computation time than basic scheduling formulations, such as deterministic or heuristic optimizations. This increased time is due to the extensive number of probabilistic scenarios considered in the stochastic approach. However, the computational burden of the stochastic scheduling formulation can be significantly alleviated by implementing suitable scenario reduction techniques. These techniques help in minimizing the number of scenarios while still capturing the uncertainty effectively, thereby enhancing the computational efficiency and overall performance of the proposed model.

4. Conclusion

This paper introduces an innovative computational framework aimed at enhancing the FFR capabilities of smart flexible loads in renewable-rich grids. By forecasting demand and RES, and estimating the net load, the study presents a stochastic scheduling model constrained by FFR requirements. The findings illustrate that FFR-constrained stochastic scheduling approach effectively optimizes flexible load operations. It not only accommodates the inherent variability of renewable energy but also ensures that grid frequency remains within acceptable bounds. The method significantly improves frequency security indicators such as RoCoF and frequency deviation, supporting the transition towards a more sustainable and resilient energy system. Cost analysis indicates that while operation costs decrease with higher RES penetration, the overall cost increase due to FFR constraints is only 0.3%. Renewable energy curtailment is reduced by 18% and achieved a 15% reduction in operation cost using flexible loads. Future research could be enhanced by incorporating challenges to incorporate EV charging infrastructure constraints, user behavior, and impacts on EV battery health.

CRediT authorship contribution statement

Ashish Mathur: Writing – review & editing, Writing – original draft, Methodology, Formal analysis, Conceptualization. **Sumit Nema:** Writing – original draft, Visualization, Software, Resources. **Vivek Prakash:** Writing – review & editing, Validation, Supervision, Software, Formal analysis, Conceptualization. **Jyotsna Singh:** Writing – review & editing, Validation, Supervision, Resources, Methodology, Investigation, Formal analysis, Conceptualization.

Declaration of competing interest

Authors do not have any conflict of interest.

Data availability

No data was used for the research described in the article.

References

[1] V. Prakash, H. Pandzic, Fast frequency control service provision from active neighborhoods: opportunities and challenges, Electr. Power Syst. Res. 217 (2023) 109161.
[2] D. Fernández-Muñoz, J.I. Pérez-Díaz, I. Guisández, M. Chazarra, Á. Fernández-Espina, Fast frequency control ancillary services: An international review, Renew. Sustain. Energy Rev. 120 (2020) 109662.
[3] D. Pieńkowski, Rethinking the concept of prosuming: A critical and integrative perspective, Energy Res. Soc. Sci. 74 (2021) 101967.
[4] J. Leitao, P. Gil, B. Ribeiro, A. Cardoso, A survey on home energy management, IEEE Access 8 (2020) 5699–5722.
[5] R. Faia, J. Soares, T. Pinto, F. Lezama, Z. Vale, J.M. Corchado, Optimal model for local energy community scheduling considering peer to peer electricity transactions, IEEE Access 9 (2021) 12420–12430.
[6] N. Rezaei, M. Kalantar, Smart microgrid hierarchical frequency control ancillary service provision based on virtual inertia concept: An integrated demand response and droop controlled distributed generation framework, Energy Convers. Manage. 92 (2015) 287–301.
[7] Y. Wen, W. Li, G. Huang, X. Liu, Frequency dynamics constrained unit commitment with battery energy storage, IEEE Trans. Power Syst. 31 (6) (2016) 5115–5125.
[8] N.B. Arias, S. Hashemi, P.B. Andersen, C. Træholt, R. Romero, Assessment of economic benefits for ev owners participating in the primary frequency regulation markets, Int. J. Electr. Power Energy Syst. 120 (2020) 105985.
[9] R. Bhana, T.J. Overbye, The commitment of interruptible load to ensure adequate system primary frequency response, IEEE Trans. Power Syst. 31 (3) (2015) 2055–2063.
[10] C. Marcus-Møller, Demand as frequency controlled reserve.
[11] Z. Xu, J. Ostergaard, M. Togeby, Demand as frequency controlled reserve, IEEE Trans. Power Syst. 26 (3) (2010) 1062–1071.
[12] P. Warren, A review of demand-side management policy in the uk, Renew. Sustain. Energy Rev. 29 (2014) 941–951.
[13] Q. Hong, Enhanced frequency control capability (efcc) project, in: CIGRE UK Next Generation Network 10 Year Anniversary Event, 2017.
[14] J. Sharma, V. Prakash, R. Bhakar, Interruptible load constrained primary frequency response scheduling with photovoltaic generation, in: 2018 20th National Power Systems Conference, NPSC, IEEE, 2018, pp. 1–6.
[15] M. Rezkalla, A. Zecchino, S. Martinenas, A.M. Prostejovsky, M. Marinelli, Comparison between synthetic inertia and fast frequency containment control based on single phase evs in a microgrid, Appl. Energy 210 (2018) 764–775.
[16] M. Marinelli, S. Martinenas, K. Knezović, P.B. Andersen, Validating a centralized approach to primary frequency control with series-produced electric vehicles, J. Energy Storage 7 (2016) 63–73.
[17] F. Teng, Y. Mu, H. Jia, J. Wu, P. Zeng, G. Strbac, Challenges on primary frequency control and potential solution from evs in the future gb electricity system, Appl. Energy 194 (2017) 353–362.
[18] A. Wangsupphaphol, N.R.N. Idris, A. Jusoh, N.D. Muhamad, S. Chaitusaney, Design and development of auxiliary energy storage for battery hybrid electric vehicle, J. Energy Storage 51 (2022) 104533.
[19] K.C. Sharma, V. Prakash, Impact of accurate forecasting on optimal operation of power system, in: Optimal Planning and Operation of Distributed Energy Resources, Springer, 2023, pp. 153–173.
[20] E.L. Karfopoulos, K.A. Panourgias, N.D. Hatziargyriou, Distributed coordination of electric vehicles providing v2 g regulation services, IEEE Trans. Power Syst. 31 (4) (2015) 2834–2846.
[21] C. O'Malley, L. Badesa, F. Teng, G. Strbac, Frequency response from aggregated v2 g chargers with uncertain ev connections, IEEE Trans. Power Syst. (2022).
[22] F. Sanchez Gorostiza, F. Gonzalez-Longatt, J.L. Rueda, Multi-objective optimal provision of fast frequency response from ev clusters, IET Gener. Transmiss. Distrib. 14 (23) (2020) 5580–5587.
[23] P. Kushwaha, V. Prakash, S. Yamujala, R. Bhakar, Fast frequency response constrained electric vehicle scheduling for low inertia power systems, J. Energy Storage 62 (2023) 106944.
[24] C. O'Malley, M. Aunedi, F. Teng, G. Strbac, Value of fleet vehicle to grid in providing transmission system operator services, in: 2020 Fifteenth International Conference on Ecological Vehicles and Renewable Energies, EVER, IEEE, 2020, pp. 1–8.
[25] V. Prakash, K.C. Sharma, R. Bhakar, H.P. Tiwari, F. Li, Frequency response constrained modified interval scheduling under wind uncertainty, IEEE Trans. Sustain. Energy 9 (1) (2017) 302–310.
[26] H. Pandžić, Y. Dvorkin, T. Qiu, Y. Wang, D.S. Kirschen, Toward cost-efficient and reliable unit commitment under uncertainty, IEEE Trans. Power Syst. 31 (2) (2015) 970–982.
[27] K. Paul, N. Kumar, S. Agrawal, Optimal rescheduling of real power to mitigate congestion with incorporation of wind farm using gravitational search algorithm in deregulated environment, Int. J. Renew. Energy Res. (IJRER) 7 (4) (2017) 1731–1740.
[28] S.V. Sah, V. Prakash, P.K. Pathak, A.K. Yadav, Virtual inertia and intelligent control assisted frequency regulation of time-delayed power system under dos attacks, Chaos Solitons Fractals 188 (2024) 115578.
[29] K. Paul, P. Sinha, Y. Bouteraa, P. Skruch, S. Mobayen, A novel improved manta ray foraging optimization approach for mitigating power system congestion in transmission network, IEEE Access 11 (2023) 10288–10307.
[30] K. Paul, V. Shekher, N. Kumar, V. Kumar, M. Kumar, Influence of wind energy source on congestion management in power system transmission network: a novel modified whale optimization approach, Process Integr. Optim. Sustain. 6 (4) (2022) 943–959.
[31] V. Prakash, K.C. Sharma, R. Bhakar, H. Tiwari, Modified interval-based generator scheduling for pfr adequacy under uncertain pv generation, IET Gener. Transm. Distrib. 13 (16) (2019) 3725–3733.
[32] K. Paul, Multi-objective risk-based optimal power system operation with renewable energy resources and battery energy storage system: A novel hybrid modified grey wolf optimization–sine cosine algorithm approach, Trans. Inst. Meas. Control (2022) 01423312221079962.
[33] P. Kushwaha, V. Prakash, R. Bhakar, U.R. Yaragatti, Pfr constrained energy storage and interruptible load scheduling under high re penetration, IET Gener. Transm. Distrib. 14 (15) (2020) 3070–3077.
[34] V. Prakash, K.C. Sharma, R. Bhakar, Optimal generation mix for frequency response adequacy in future power system, Energy Built Environ. 2 (3) (2021) 243–250.
[35] H.H. Çoban, Interaction of local flexibility with national ancillary services markets: Paving the way for türkiye's sustainable grid, Turkish J. Electr.Power Energy Syst. (2024).
[36] P. Kushwaha, V. Prakash, R. Bhakar, A novel framework to assess synthetic inertia & primary frequency response support from energy storage systems, Sustain. Energy Grids Netw. 34 (2023) 101052.
[37] H.H. Coban, M. Bajaj, A. Rajagopalan, D. Swaminathan, A. Oubelaid, Revenue analysis of cooperation of battery storage and wind power to provide frequency regulation in the energy market, in: 2023 4th IEEE Global Conference for Advancement in Technology, GCAT, IEEE, 2023, pp. 1–7.
[38] K. Paul, D. Hati, A novel hybrid harris hawk optimization and sine cosine algorithm based home energy management system for residential buildings, Build. Serv. Eng. Res. Technol. 44 (4) (2023) 459–480.
[39] A. Mathur, S. Nema, V. Prakash, J. Singh, Demand response strategy from delay and non-linearity constrained electric vehicles, in: 2023 IEEE 2nd International Conference on Industrial Electronics: Developments & Applications, ICIDeA, IEEE, 2023, pp. 427–432.

[40] S. Chawda, V. Prakash, Impact assessment of solar integrated residential consumers on retailer decision-making, Smart Grids Sustain. Energy 8 (3) (2023) 14.
[41] S. Nema, V. Prakash, H. Pandžić, Frequency-responsive refrigerator switching controller, IEEE Trans. Smart Grid (2023).
[42] A. Mathur, V. Prakash, J. Singh, T. Rawat, Capacity planning of wind farm to simultaneously optimize hosting capacity and losses in distribution system with electric vehicles, Electr. Power Syst. Res. 229 (2024) 110159.
[43] A. Soroudi, Possibilistic-scenario model for dg impact assessment on distribution networks in an uncertain environment, IEEE Trans. Power Syst. 27 (3) (2012) 1283–1293.
[44] A. Ali, K. Mahmoud, M. Lehtonen, Optimization of photovoltaic and wind generation systems for autonomous microgrids with pev-parking lots, IEEE Syst. J. 16 (2) (2021) 3260–3271.
[45] J. Singh, R. Tiwari, Cost benefit analysis for v2 g implementation of electric vehicles in distribution system, IEEE Trans. Ind. Appl. 56 (5) (2020) 5963–5973.
[46] H. Heitsch, W. Römisch, Scenario reduction algorithms in stochastic programming, Comput. Optimiz. Appl. 24 (2003) 187–206.
[47] V. Prakash, R. Bhakar, H. Tiwari, K.C. Sharma, System inertia prediction for primary frequency response adequacy under uncertain wind generation, in: 2018 8th IEEE India International Conference on Power Electronics, IICPE, IEEE, 2018, pp. 1–6.
[48] R.T. Force, Ieee reliability test system, IEEE Trans. PAS 98 (6) (1979) 2047–2054.

Ashish Mathur He is currently pursuing the Ph.D. degree with Banasthali Vidyapith, Tonk, Rajasthan, India. He is working as an Assistant Professor in the school of automation, Banasthali Vidyapith. His research interests include power system ancillary services planning, operation, control, and economics of power and energy systems.

Sumit Nema (Student Member, IEEE) received the B.E. and M.E. degrees from the Rajiv Gandhi Proudyogiki Vishwavidyalaya, Bhopal, Madhya Pradesh, India, in 2010 and 2015, respectively. He is currently pursuing the Ph.D. degree with Banasthali Vidyapith, Tonk, Rajasthan, India. His research interests include power system ancillary services planning, operation, control, and economics of power and energy systems.

Vivek Prakash (Senior Member, IEEE) received the Ph.D. degree in electrical engineering from the Malaviya National Institute of Technology Jaipur, India, in 2019 and PDF from University of Zagreb Faculty of electrical engineering and computing. He is currently working as an assistant professor at Banasthali Vidyapith, Rajasthan, India. His research interests include operations, control, and economics of power and energy systems.

Jyotsna Singh (Member, IEEE) received the B.E. degree in electrical engineering from the Maharana Pratap University of Agriculture and Technology, Udaipur, Rajasthan and the M.Tech., Ph.D. degree in power systems and Electrical Engineering respectively from the Malaviya National Institute of Technology (MNIT), Jaipur, Rajasthan. She is currently working as an assistant professor at Banasthali Vidyapith, Rajasthan, India. Her area of interest includes electric vehicles, distributed energy resources, smart grid operation.